Effect of cold wire addition in tandem submerged arc welding on weld geometry and micro-hardness of heavy gauge X70 steel

Tailin Ren[1,*], Mohsen Mohammadijoo[2], J Barry Wiskel[1], Robert Lazor[3], Eric Willett[3], Douglas G. Ivey[1], Hani Henein[1]

[1] Department of Chemical and Materials Engineering, University of Alberta, Edmonton, AB, Canada T6G2V4

[2] Formerly with R&D Division, EVRAZ Inc. NA, P.O. Box 1670, Regina, SK, Canada S4P 3C7

[3] TC Energy Corporation, Calgary, AB, Canada T2P 5H1

Abstract

The pipeline industry has undertaken an essential upgrade of well established X70 pipeline steel in heavy gauge pipes to fill the demand of increased operating pressures. A developed welding process, cold wire tandem submerged arc welding (CWTSAW), with improved deposition rate and travel speed can meet this upgrade. Currently, the effect of CWTSAW process parameters and bevel design on the change in weld geometry and properties of the weld and heat-affected zone (HAZ) in heavy gauge X70 pipe is not well understood. In this article, a series of weld trials were conducted on heavy gauge (19.1 mm) X70 steel plates to investigate the effect of cold wire feed speed, heat input and bevel design on the reinforcement size, coarse grained heat-affected zone (CGHAZ) area, ratio of weld shapes and micro-hardness of the weld and HAZ. The results showed that the cold wire feed speed significantly influenced the micro-hardness profiles, and bevel design was the dominant factor influencing the reinforcement size and CGHAZ area. In addition, empirical equations of micro-hardness profiles of the CWTSAW samples were developed using a non-linear regression analysis. The phase fraction and morphology of martensite-austenite (MA) constituents were analyzed using optical microscopy and scanning electron microscopy. The microstructural results indicated lower MA fractions with fine and dispersed MA constituents obtained in the CGHAZ of the CWTSAW samples than for conventional tandem submerged arc welding samples. This can be interpreted as the reason for the lower hardness in the CGHAZ of the CWTSAW samples.

Keywords

Cold wire tandem submerged arc welding, Microalloyed pipeline steel, Taguchi method, Micro-hardness, Weld geometry

* Corresponding author: Tailin Ren (tailin@ualberta.ca)

Acronyms

ACSQ	Square wave alternating current	ICHAZ	Inter-critical heat-affected zone
ANOVA	Analysis of variance	LBZ	Localized brittle zone
AR	Aspect ratio	MA	Martensite-austenite
BA	Bevel area	OM	Optical microscopy
BD	Bevel design	PA	Penetration area
BM	Base metal	PD	Penetration depth
BTA	Bead toe angle	RA	Reinforcement area
BW	Bead width	S/N	Signal-to-noise
$BW_{1/2}$	Bead width at half of penetration	SAW	Submerged arc welding
CGHAZ	Coarse grained heat-affected zone	SE	Secondary electron
CWFS	Cold wire feed speed	SEM	Scanning electrode microscopy
CWTSAW	Cold wire tandem submerged arc welding	SPR	Semi-penetration ratio
DCEP	Direct current electrode positive	TMCP	Thermo-mechanical controlled processing
DIL	Dilution	TOMR	Three order multiple regression
FGHAZ	Fine grained heat-affected zone	TS	Travel speed
HAZ	Heat-affected zone	TSAW	Tandem submerged arc welding
HI	Nominal heat input	V	Voltage
HIL	Nominal heat input of the lead electrode	VL	Voltage of the lead electrode
HIT	Nominal heat input of the trail electrode	VT	Voltage of the trail electrode
HRA	Height of the reinforcement area	WM	Weld metal

Notation

DF	Degrees of freedom
F	Variance ratio
R^2	Coefficient of determination
SS	Sum of squares
η	Arc efficiency
ρ	Effective contribution

1.0 Introduction

Production of heavy gauge (>16 mm wall thickness) X70 pipe is a recent focus in pipeline manufacturing to achieve the requirement of increased operating pressures [1]. As one of the manufacturing processes, submerged arc welding (SAW) offers substantial benefits, including high deposition rate, deep penetration and reduced welding times. These attributes are beneficial for welding heavy gauge plates [1, 2]. To increase productivity of heavy gauge pipes, tandem submerged arc welding (TSAW) containing two or more electrodes has been developed for the welding procedure of line pipe to achieve a high deposition rate [3]. The use of multi-electrode TSAW may, however, result in an increase in overall heat input which affects the metallurgy/properties of the weld metal (WM) and heat-affected zone (HAZ), especially in the coarse grained heat-affected zone (CGHAZ). Consequently, the quality of weldments, such as toughness and microstructure, may deteriorate [4, 5]. To increase productivity while maintaining the quality of TSAW pipeline products, cold wire tandem submerged arc welding (CWTSAW) was developed [6, 7].

CWTSAW is defined as a TSAW process where an additional electrode with no arc is introduced within the molten pool. The primary objective of involving a cold wire is to increase the deposition rate and decrease the overall heat input into the weld. This method was first developed by Mruczek et al. [6] in the SAW process for enhancing welding capabilities and improving weld productivity by increasing deposition rate. Ramakrishnan et al. [8] utilized three wires and cold wire addition in SAW welds and these contributed to a 30% increases in weld toughness relative to a conventional three wire process. Júnior RC et al. [9] reported that feeding a cold wire in the multiple wire SAW process of a duplex stainless steel with a heat input of 2.7 kJ/mm resulted in increased corrosion resistance due to a decreased HAZ width and increased

austenite phase fraction. Previous studies [7, 10, 11] applied CWTSAW to an intermediate gauge X70 line pipe (13.4 mm thick) and showed a 17% reduction in overall heat input and a 12% increase in deposition rate with improved fracture toughness which enhanced productivity of intermediate gauge X70 line pipe welding. In the pursuit of promising welding techniques with cold wire addition, the levels of heat input (HI) and cold wire feed speed (CWFS), in contrast to previous work [7], need to be increased for the production of heavy gauge X70 line pipe (19.1 mm thick). Adjustments to the levels of welding process parameters and bevel geometry can cause significant change in the resulting geometry for the weld and HAZ [2]. Furthermore, the microstructure and properties of the weld are influenced by the composition of the WM and weld shape [12]. In the pipeline industry, a qualified weld geometry can be described as the shape with deep penetration and smaller HAZ area at lower heat inputs [7, 12]. Therefore, it is necessary to design an experiment to study the effect of CWTSAW process parameters and bevel design on the change in weld geometry and micro-hardness profiles of heavy gauge X70 steel.

The Taguchi design is a statistical technique used to design an experiment and optimize manufacturing process parameters [13]. This method has been widely used in numerous studies to optimize the welding process. Tarng and Yang [14] determined the optimal welding parameters of the SAW process with a small number of tests utilizing Taguchi design. Sarkar et al. [15] employed Taguchi design to analyze the effective contribution of bead geometry on tensile strength and validated the results with confirmatory tests in the SAW process. The weld geometry and micro-hardness measurements from the Taguchi design were analyzed using three statistical methods; i.e., analysis of variance (ANOVA), three order multiple regression (TOMR) analysis and signal-to-noise (S/N) ratio. ANOVA was used to determine the significant weld parameters by analyzing the variability of the data using the variance ratio (F value), sum of squares (SS) and level of

significance (P value) [16]. TOMR analysis is a nonlinear model used to develop empirical equations for response characteristics and mechanical properties, such as the CGHAZ area and micro-hardness of the CGHAZ and WM [17]. S/N ratio is the method for optimizing the levels of weld parameters to improve weld geometry [18].

In this study, the CWTSAW process was applied to heavy gauge (19.1 mm thick) X70 line pipe steel. The effects of heat input of the lead (HIL) and trail (HIT) electrodes, voltage of the lead (VL) and trail (VT) electrodes, travel speed (TS), bevel design (BD), and cold wire feed speed (CWFS) on the weld geometry, hardness of the HAZ and microstructural modification in the CGHAZ were studied. In total, 16 test welds were conducted. The specific test welds were designed using the Taguchi method. Following welding, the weld geometrical characteristics were measured including the reinforcement area (RA), the height of the reinforcement area (HRA), bead toe angle (BTA), aspect ratio (AR), semi-penetration ratio (SPR), and coarse grained heat-affected zone (CGHAZ) area. In addition, the amount of weld dilution (DIL) and the micro-hardness of the CGHAZ and WM were measured. Finally, a comparison of martensite-austenite (MA) constituents in the CGHAZ of the conventional TSAW and CWTSAW processes was undertaken using optical microscopy (OM) and scanning electron microscopy (SEM).

2.0 Experimental Methods

2.1 Base and Electrode Material

The CWTSAW weld tests were conducted on heavy gauge (19.1 mm thick) X70 microalloyed steel. The composition of the X70 steel is shown in Table 1. The studied X70 microalloyed steel was fabricated through thermo-mechanical controlled processing (TMCP) [1].

The electrodes used in the study for both hot wires and the cold wire were selected based on EN14295/EN 756. A 4 mm diameter S2Mo solid wire was selected for the electrodes and cold wire. The compositions are shown in Table 1.

Table 1 Composition of X70 microalloyed steel and electrode (wt. %)

X70 Composition								
C	P	S	Mn	Si	N	V+Mo+Ti+Nb	Cu+Ni+Cr+Al+Ca	Fe
0.04	0.01	0.003	1.32	0.28	0.007	0.34	0.63	97.37
Electrode and cold-wire composition (S2Mo)								
C	P	S	Mn	Si	Mo	Ni	Cr	Cu
0.1	0.007	0.01	1.04	0.1	0.56	0.02	0.03	0.03

2.2 Weld Bevel Specifications

Weld samples were fabricated and machined with two different bevel designs. Figure 1 compares the two bevel types used. Each bevel is generated on the same thickness of skelp, but the cross-sectional areas are different. For instance, the 60° bevel with a 4.5 mm depth has a 12 mm^2 cross-sectional area, while the 90° bevel with a 5 mm depth has a larger cross-sectional area of 25 mm^2. The quantitative description of the bevel specification is convenient for the representation of the two bevel types in statistical analysis.

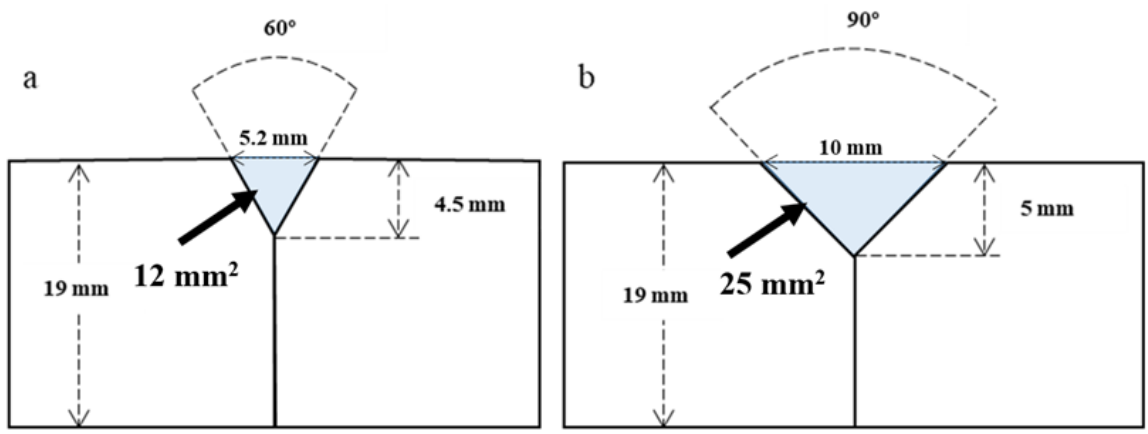

Figure 1 Schematic view of bevel specifications.

2.3 CWTSAW Setup

Three electrodes (lead, trail and cold electrode) were fed into the molten pool, as illustrated in Figure 2a. The electrically cold electrode is located at a lagging position relative to the trail electrode. The electrode setup is shown in Figure 2b, including the stick out length (25 mm), electrode separation (13 mm) and the angular position of each electrode relative to a normal to the skelp surface. The constant power sources of the lead and trail electrodes were direct current electrode positive (DCEP) polarity and square wave alternating current (ACSQ) polarity, respectively. There was no power source for the cold electrode. As a basic feature in SAW, a consumable granular flux is needed to shield the welding pool and to fill the bevel area. According to EN 760, BF6.5 consumable flux was used in the CWTSAW process.

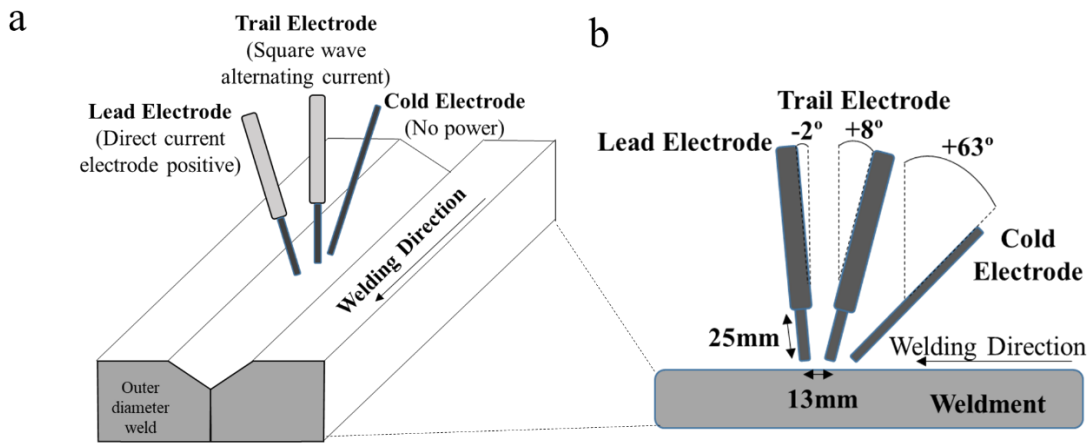

Figure 2 Setup for CWTSAW process: a) Overview of welding set up, b) schematic view of fixed welding variables.

2.4 Welding Parameters

The four fundamental welding parameters are current, voltage, travel speed and feed speed of the electrodes. For the CWTSAW process, there are additional welding parameters based on the use of multiple electrodes. However, in order to understand the effect of heat input on the

weldments and to keep the number of welding tests manageable, the current of the lead and trail electrodes was not varied independently and the feed speed of the trail and lead electrodes was kept constant. The nominal heat input (HI) and voltage (V) are key welding parameters and the current was calculated and set during welding according to Equation 1 [7].

$$\mathrm{HI}\left(\frac{\mathrm{kJ}}{\mathrm{mm}}\right) = \frac{\eta \cdot V \cdot I}{1000 \cdot TS} \quad (1)$$

Where HI, V, I and TS represent nominal heat input, voltage, current and travel speed. The arc efficiency (η) is in the range of 0.9-1.0 for SAW [7].

Seven welding parameters with mixed levels, including five main welding parameters such as heat input and voltage of lead and trail electrodes and travel speed, were selected for CWTSAW tests. These are shown in Table 2. The heat input, voltage and travel speed are fundamental and crucial parameters for a welding process and need to be included. Moreover, the cold wire parameter and bevel specification parameter are CWFS and BD, respectively. CWFS and BD were selected to study the effect of the cold wire addition and varied bevel types on weld characteristics and hardness. Only CWFS is a four-level welding parameter, while the others are two-level.

Table 2 CWTSAW tests parameters and input levels

Symbol	Process parameter	Notation	Unit	Level 1	Level 2	Level 3	Level 4
A	Cold wire feed electrode	CWFS	mm/s	16.9	25.4	33.9	42.3
B	Heat input of lead electrode	HIL	kJ/mm	1.6	1.8	-	-
C	Heat input of trail electrode	HIT	kJ/mm	1.3	1.5	-	-
D	Voltage of lead electrode	VL	V	33	36	-	-
E	Voltage of lead electrode	VT	V	34	37	-	-
F	Travel speed	TS	mm/s	21.2	23.3	-	-
G	Bevel design	BD	mm^2	12	25	-	-

2.5 Experimental Table

Taguchi analysis was employed for the parametric study of CWTSAW. The main advantage of Taguchi analysis is the use of a small number of welding tests, which is more economical and effective than using a factorial design [13]. Based on six parameters with two levels and one parameter with four levels, an L16 orthogonal array was designed using Taguchi analysis and is shown in Table 3. The L16 array comprised 16 weld tests and each level of the parameters appears the same number of times in each column. The weld geometrical values were measured for all 16 weld tests and analyzed using statistical methods. Additionally, a welding table of three validation tests is shown in Table 4. These tests were used to validate the linear trend between the measured and predicted results in the TOMR analysis.

Table 3 L16 orthogonal array based on Taguchi analysis

Test no.	A(CWFS) (mm/s)	B(HIL) (kJ/mm)	C(HIT) (kJ/mm)	D(VL) (V)	E(VT) (V)	F(TS) (mm/s)	G(BD) (mm^2)
1	16.9	1.6	1.3	33	34	21.2	12
2	16.9	1.6	1.3	33	34	23.3	25
3	16.9	1.8	1.5	36	37	21.2	12
4	16.9	1.8	1.5	36	37	23.3	25
5	25.4	1.6	1.3	36	37	21.2	12
6	25.4	1.6	1.3	36	37	23.3	25
7	25.4	1.8	1.5	33	34	21.2	12
8	25.4	1.8	1.5	33	34	23.3	25
9	33.9	1.6	1.5	33	37	21.2	25
10	33.9	1.6	1.5	33	37	23.3	12
11	33.9	1.8	1.3	36	34	21.2	25
12	33.9	1.8	1.3	36	34	23.3	12
13	42.3	1.6	1.5	36	34	21.2	25
14	42.3	1.6	1.5	36	34	23.3	12
15	42.3	1.8	1.3	33	37	21.2	25
16	42.3	1.8	1.3	33	37	23.3	12

Table 4 Welding conditions for validation tests

Test no.	A(CWFS) (mm/s)	B(HIL) (kJ/mm)	C(HIT) (kJ/mm)	D(VL) (V)	E(VT) (V)	F(TS) (mm/s)	G(BD) (mm^2)
C1	25.4	2.0	1.4	36	34	21.2	25
C2	33.9	1.6	1.8	33	37	21.2	25
C3	29.6	1.8	1.4	33	38	21.2	25

2.6 Weld Characteristics

Three weld samples extracted from each weldment, as shown in Figure 3a, were used to measure geometry characteristics. A vertical band saw, assisted with coolant, was employed in sectioning. A total of 48 specimens was examined. Each sample was mounted and polished following the ASTM E3-11 standard [19] and then were macro-etched using 4% Nital to reveal the HAZ and WM boundaries (Figure 3b). A stereomicroscope image was obtained from each section and analyzed using Image J 1.52a software to obtain the weld geometry values, including bead width (BW), penetration depth (PD), penetration area (PA), bead width at half penetration depth ($BW_{1/2}$), HRA, RA, bead toe angle (BTA) and CGHAZ area, as per Figure 3b.

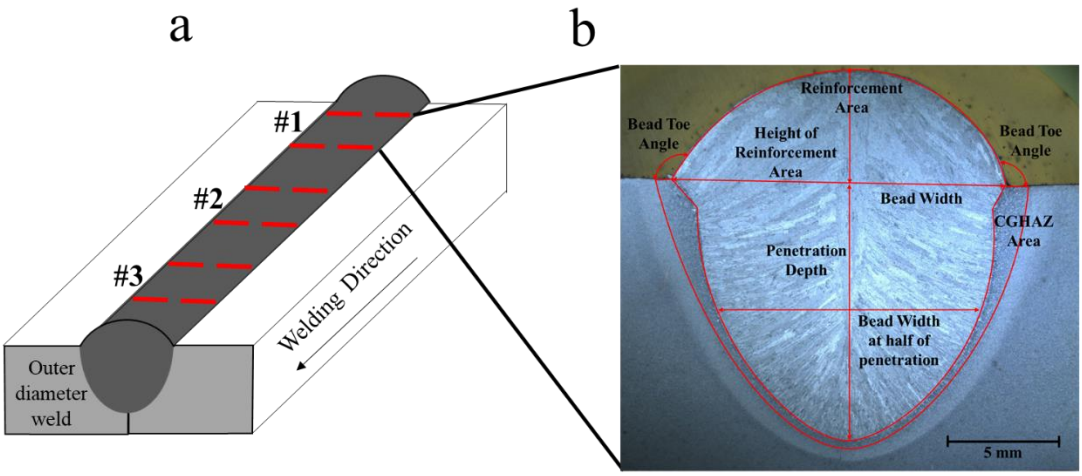

Figure 3 a) Schematic showing sectioning position of welds. b) Macrograph of Sample Test 1-1.

The weld geometry values obtained from the stereomicroscope images were utilized to calculate AR, SPR and the amount of DIL of the weld, as shown in Equations 2 to 4 [7], respectively.

$$AR = \frac{\mathrm{PD}}{\mathrm{BW}} \quad (2)$$

$$SPR = \frac{BW_{1/2}}{\mathrm{BW}} \quad (3)$$

$$DIL = \frac{\mathrm{PA-BA}}{\mathrm{PA+RA}} \quad (4)$$

The bevel areas (BA) in the two bevel specifications were 12 mm^2 and 25 mm^2 (Figure 1).

2.7 Micro-hardness

Vickers micro-hardness measurements were obtained from the BM, HAZ and WM, as illustrated in Figure 4 [20]. Two indentation lines (5 mm below the surface) contained a total of 50 indents from each weld sample to guarantee 10 to 12 indents in each of the WM and CGHAZ. A 500 g load and a dwell time of 14 s were used. The distance between two indents was three times the size of an indent, as indicated in the optical images in Figure 4.

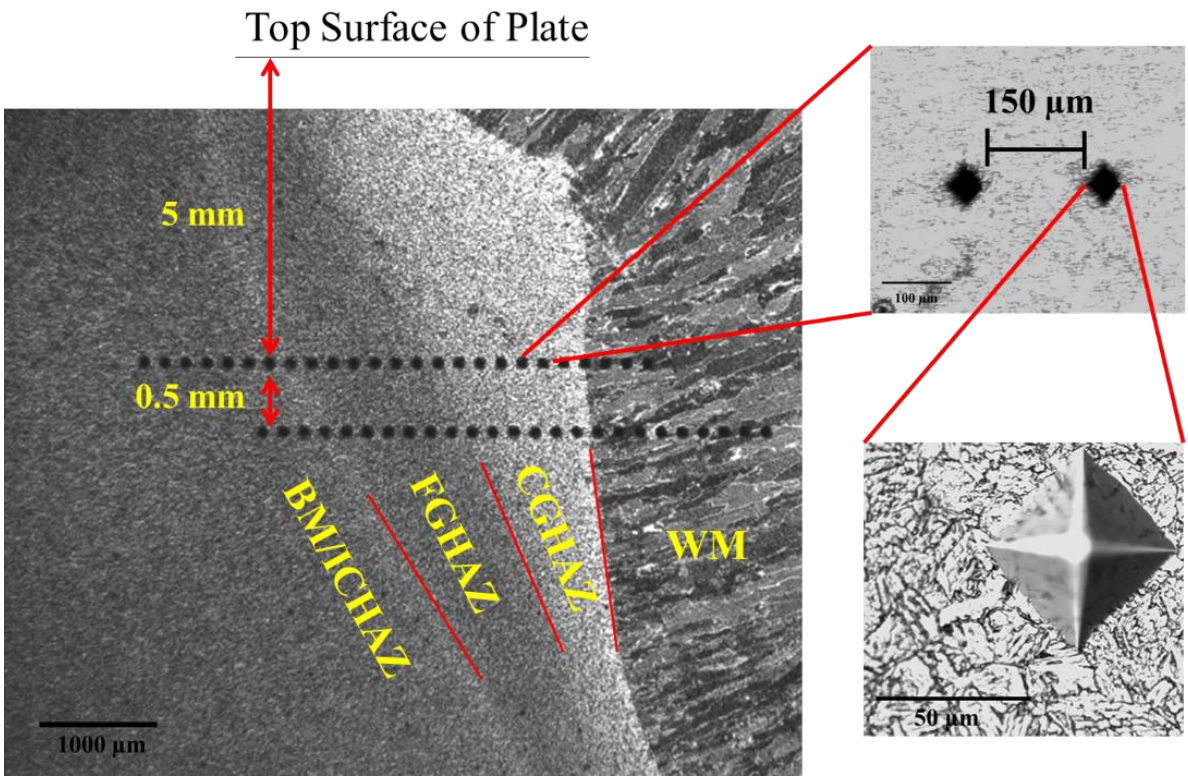

Figure 4 Schematic of the micro-hardness mapping along the HAZ and WM of Sample T1-1.

2.8 Microstructural Characterization

Optical microscopy (OM) was conducted using an Olympus BX61 microscope and Olympus StreamMotion software. Scanning electron microscopy (SEM) was done using a Zeiss EVO M10 SEM operating at 20 kV accelerating voltage. The weld specimens were micro-etched with modified LePera's solution to reveal MA constituents in the HAZ [21]. Then, three optical and three SEM secondary electron (SE) micrographs were taken from a location 5 mm below the weld surface and 50-200 µm from the fusion line. The phase fractions of MA constituents in the CGHAZ of TSAW and CWTSAW welds were measured from both optical and SEM micrographs using the color threshold feature of Image J 1.52a software.

3.0 Results

The BW, HRA, BTA, RA, CGHAZ area, CGHAZ hardness, WM hardness, PA, PD and $BW_{1/2}$ were measured for all 16 test welds. The values for each characteristic are shown in Table 5. Of particular note is the largest value of CGHAZ area (30.2 mm^2) observed for Test 8. This test had the highest heat input of all the welds. Maximum values for other characteristics are indicated in bold and minimum values are underlined in each column.

Table 5 Measured weld characteristics

Trial No.	BW (mm)	HRA (mm)	BTA (°)	RA (mm^2)	CGHAZ area (mm^2)	CGHAZ hardness (HV0.5)	WM hardness (HV0.5)	PA (mm^2)	PD (mm)	$BW_{1/2}$ (mm)
1	14.0	5.0	123.5	51.3	22.1	215.9	230.0	123.2	11.6	12.0
2	13.4	4.2	127.8	39.5	27.5	**223.8**	233.2	139.7	13.0	12.1
3	15.3	4.4	125.2	47.5	24.2	220.6	234.7	139.1	12.3	12.7
4	14.1	3.6	130.7	35.0	26.0	220.1	**237.1**	161.0	13.7	**13.5**
5	15.1	4.0	127.0	45.4	20.8	216.2	233.7	119.4	10.9	12.1
6	14.7	3.9	135.7	36.8	24.4	222.3	232.0	142.6	12.2	13.1
7	13.2	**5.7**	111.8	**57.1**	26.1	216.6	232.9	139.2	13.3	12.0
8	12.4	5.2	113.5	47.9	**30.2**	215.1	234.4	**171.4**	**15.2**	13.4
9	14.7	3.5	124.0	37.4	27.4	212.9	229.7	142.9	13.2	12.2
10	13.3	4.9	121.7	49.2	23.8	215.0	235.4	135.4	12.8	12.3
11	14.7	3.2	**136.6**	31.9	27.8	208.9	225.8	143.4	13.1	12.5
12	14.4	4.9	119.8	52.9	23.0	215.4	228.8	132.8	12.1	12.2
13	**15.6**	4.0	133.2	43.1	25.7	213.8	232.7	136.6	12.4	11.7
14	12.8	5.5	112.1	52.3	23.1	219.9	236.1	134.4	12.8	11.9
15	13.5	3.5	136.0	31.2	27.8	215.6	234.3	142.3	13.1	11.8
16	13.3	4.9	119.6	47.1	22.2	209.7	230.5	134.7	12.5	12.4

The calculated values for AR, SPR and DIL are shown in Table 6. Maximum values for each calculated characteristic are indicated in bold and minimum values are underlined in each column. The largest values of AR and SPR are for Test 8 (highest heat input). The lowest amount

of DIL is observed in Test 13. In general, a lower amount of DIL leads to better weld properties, as reported in references [22, 23].

Table 6 Calculated weld characteristics

Trial No.	1	2	3	4	5	6	7	8	9	10	11	12	13	14	15	16
AR	0.83	0.98	0.80	0.97	0.72	0.83	1.01	**1.22**	0.90	0.97	0.89	0.84	0.80	1.00	0.97	0.94
SPR	0.86	0.90	0.83	0.96	0.80	0.89	0.91	**1.08**	0.83	0.93	0.85	0.85	0.75	0.93	0.88	0.94
DIL	0.63	0.64	0.68	**0.69**	0.65	0.66	0.65	0.67	0.65	0.67	0.68	0.65	0.62	0.66	0.68	0.68

The relationship between different weld characteristics can be made to help understand the welding process. Figure 5a shows a plot of PA vs. CGHAZ area, where CGHAZ area is shown to increase as PA increases. The trend line shown is for illustrative purposes only. This indicates that as weld metal size increases (via heat input and bevel design) an accompanying increase in CGHAZ area will occur. Both Test 4 and Test 8 appear to show significant increases in PA relative to the size of the CGHAZ area. Test 8 has the highest heat input and Test 4 appears to be an outlier.

The relationship between RA and CGHAZ area is shown in Figure 5b. The CGHAZ area increases as RA decreases. The decreased RA may facilitate full penetration in the weld which may influence the size of the CGHAZ area. However, Test 7 and Test 8 do not follow the trend which may be related to their high heat input. The bevel design (BD) is also believed to influence the observed correlation between the RA and CGHAZ area. This will be discussed in Section 4.1. Additional analysis of the correlation between welding parameters and measured weld geometry is presented in Section 4.2.

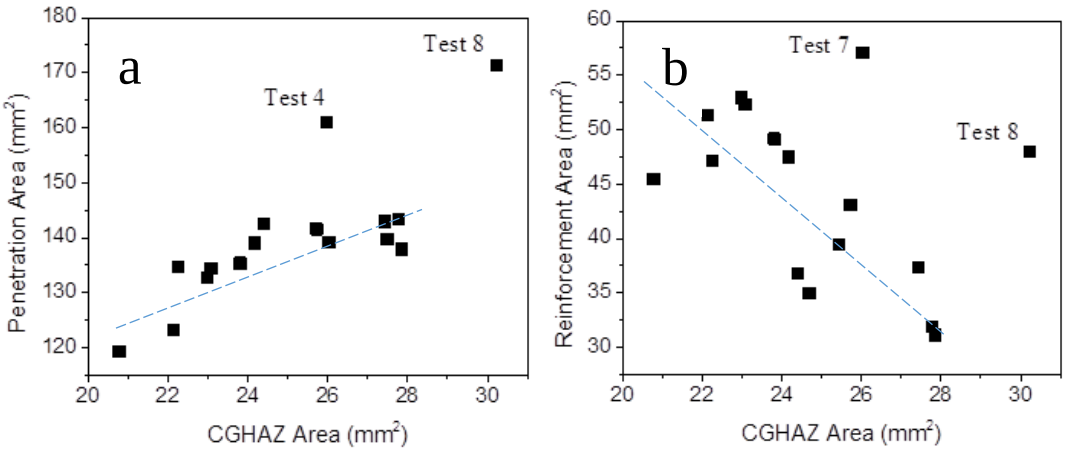

Figure 5 Plot of CGHAZ area vs. a) PA and b) RA.

4.0 Discussion

4.1 Significance of Welding Parameters

The analysis of variance (ANOVA) was carried out on the measured weld characteristics to determine the statistical significance of the welding parameters. All ANOVA tables are presented in Appendix A (Table 10) and include probabilities of significance (P), degrees of freedom (DF), sum of squares (SS), variance ratios (F) and coefficient of determination (R^2) values for each welding parameter. According to the statistical analysis reported by Mruczek et al. [6] and Shahverdi et al. [24], P values are used to determine the statistical significance of each of the welding parameters. A P value equal to or less than 0.05 indicates the parameter is statistically significant with 95% confidence. A P value of 0.25 corresponds to a 75% confidence level that the parameter is statistically significant for the weld characteristic. For this work, the significant parameters for the weld geometry results and the amount of DIL were selected based on a 95% confidence level, while a 75% confidence level was used to analyze miro-hardness values of the CGHAZ and WM. The selected significant parameters for each weld characteristic, the amount of

DIL and micro-hardness profiles are shown in Figure 6. For example, the significant welding parameters affecting RA are HIT, VT and BD, all with a confidence level of 95%. Of particular note is that BD has a significant effect on the CGAHZ area and reinforcement size (RA and BTA), but BD has only a minor influence on the micro-haradness profiles. In addition, CWFS has a dominant influence on the micro-hardness profiles in the CGHAZ and WM, but the effect of CWFS on the DIL, bead ratio values and reinforcement size is insignificant. The dominant effect of BD and CWFS on reinfrocement size and micro-hardness profiles will be discussed when the analysis of effective distribution is considered.

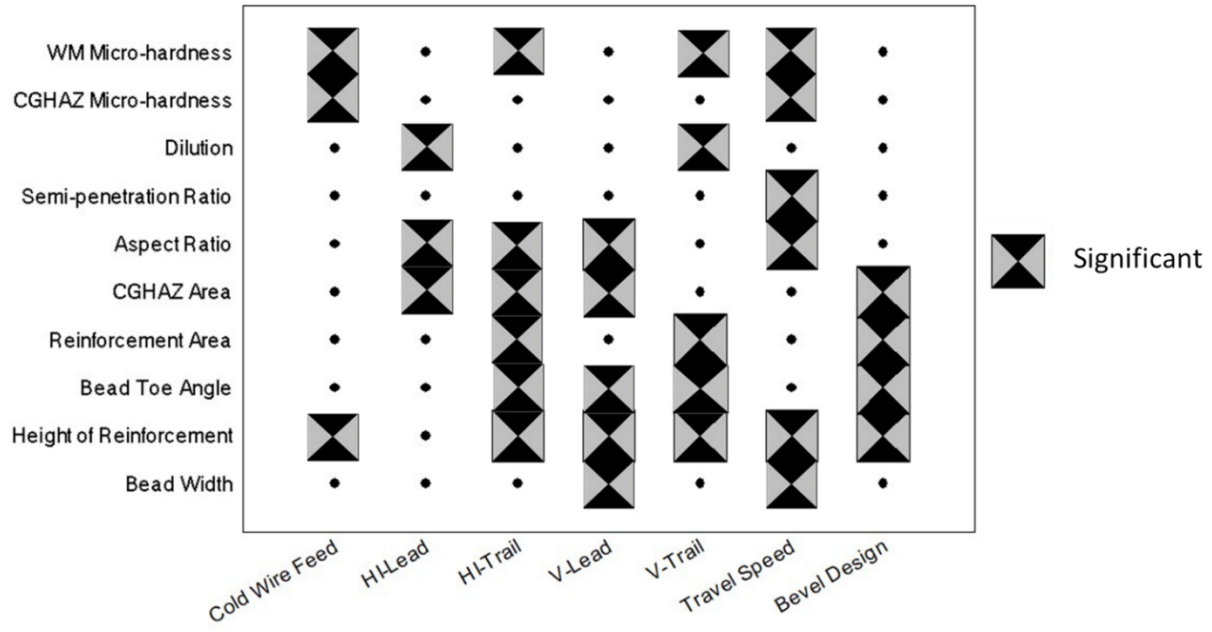

Figure 6 Significant welding parameters for weld geometry, DIL and the micro-hardness of WM and CGHAZ.

The most significant welding parameter was decided for each weld geometry result and micro-hardness profile using the effective contribution (ρ). The effective contribution of each parameter depends on the sum of squares, which is the deviation from the total average value of

population. The concept of effective contribution is a fundamental term in ANOVA analysis and can be calculated by Equation 5 [16].

$$\rho(\%) = \frac{SS_i}{SS_t} \cdot 100\% \quad (5)$$

where ρ is the effective contribution of each parameter to the response characteristics and SS_i and SS_t are the sum of squares for each parameter and the total sum of squares, respectively. The contribution evaluates the importance of parameters on each weld characteristic and the WM and CGHAZ micro-hardness. The significant contributions for BW, AR, DIL and SPR are shown in Figure 7.

Overall voltage (lead + trail electrodes) and TS significantly influence BW, AR and SPR, as shown in Figure 7. It is generally accepted that a higher arc voltage leads to a wider arc length promoting the formation of a wide BW [2, 25, 26]. Pepin et al. [26] correlated TS with penetration profile of intermediate gauge strip and reported that a high TS reduces the filler metal per unit length of weld leading to a narrow weld. Specifically, a faster TS and lower V result in a shorter arc length and, as such, a smaller BW. The AR and SPR were calculated using Equations 2 and 3. Both geometric ratio results are significantly affected by VL and TS. An increasing TS results in a smaller BW due to the reduced heat input and reduced melted metal per unit length [25]. Therefore, both AR and SPR are affected by voltage and TS, due to the change in BW.

DIL is defined as the ratio of the amount of adjacent metal melted to the total amount of fused metal. As such, the amount of dilution can be calculated by using two geometric results, PA and RA, as expressed in Equation 4. In Figure 7, the maximum effective contribution for welding parameters on DIL is 39.1 % for HIL. This finding is correlated with the polarity of the electrode and weld penetration depth. The use of positive polarity can increase penetration depth and area since additional base metal is melted [25, 26]. In this study, the polarity of the HIL is selected as

DCEP in the welding process. Therefore, a higher HIL increases the penetration depth leading to more DIL. Finally, it is common to minimize the amount of dilution since the amount of dilution affects the composition of the molten pool and the resultant mechanical properties in the welds [7, 27].

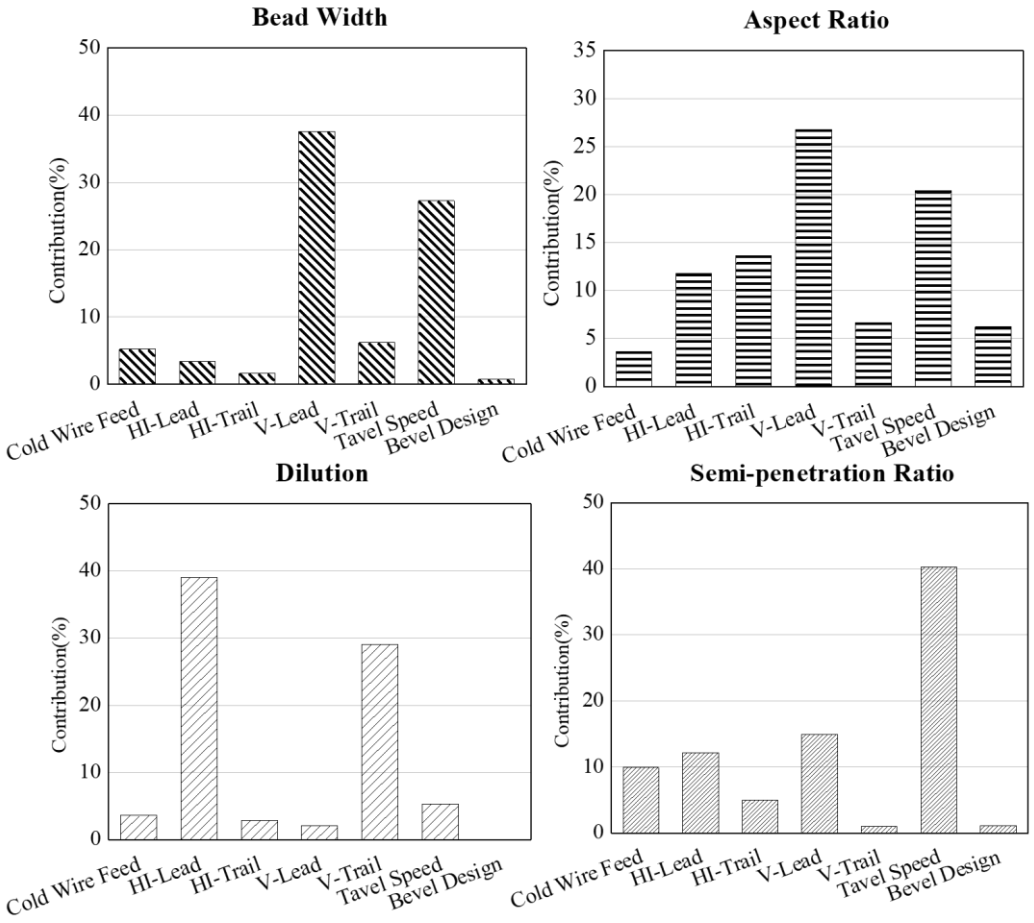

Figure 7 Effective contributions of CWTSAW process parameters for BW, AR, DIL and SPR.

Figure 8 shows that the CWFS has the most dominant effect on the CGHAZ and WM micro-hardness profiles, since cold wire addition alters the local thermal cycle by consuming heat from the molten pool. In addition, the heat input and voltage may contribute to the CGHAZ hardness profile since they can change the local thermal cycle and size of the CGHAZ area. It is difficult to compare the effects of CWFS on hardness when other parameters are varied as well.

Therefore, nonlinear relationship analysis between interactions of welding parameters and micro-hardness profiles in the CGHAZ and WM is necessary and is discussed in Subsection 4.2.

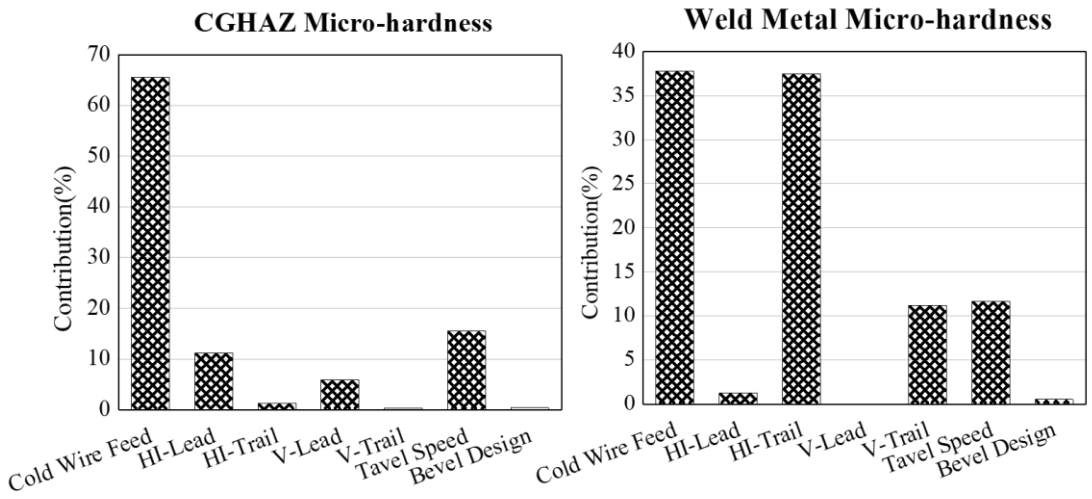

Figure 8 Effective contribution of CWTSAW process parameters for the WM and CGHAZ micro-hardness.

In Figure 9, HIL is less effective for reinforcement regions (HRA, RA and BTA) since the positive polarity of HIL is more dominant for the penetration profiles. However, BD showed the greatest effective contribution on HRA, BTA, CGHAZ area and RA. In order to understand the effect of BD, the 16 measurements of RA, HRA, BA, and CGHAZ area were plotted against the two bevel specifications separately, as shown in Figure 10. The BD with a wider bevel area had lower RA and HRA, and increased BTA and CGHAZ area. This means that smaller and shallower reinforcement regions were produced for the larger bevel angle. It is generally accepted that larger bevel angle and depth lead to a larger bevel area promoting more molten metal flowing downward. The heat transformation from the top to the bottom of the weld resulted in full penetration. Therefore, this achievement of full penetration caused a smaller RA in the wider BD. These findings are consistent with the results in the simulation of Chen et al. [28] and the tungsten inert gas welding results of Huang et al. [29].

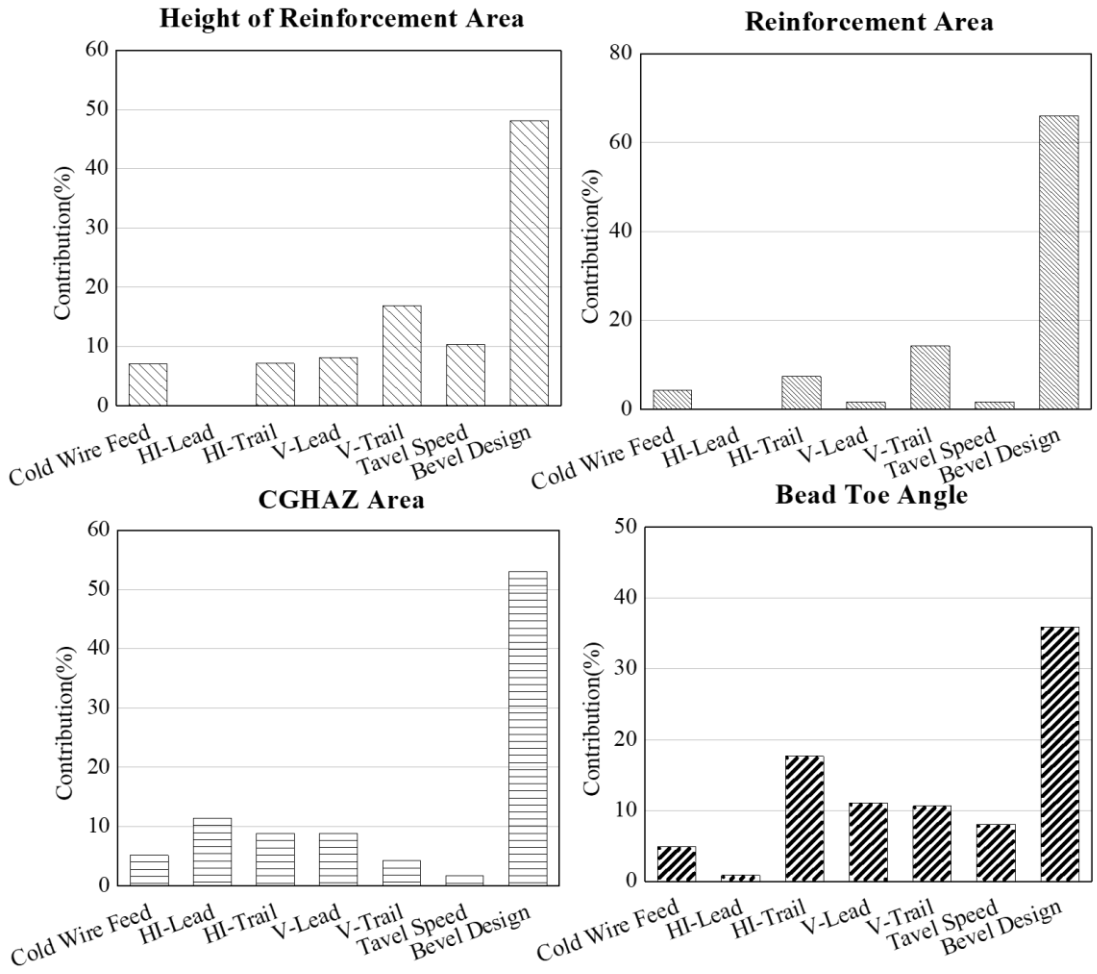

Figure 9 Effective contribution of CWTSAW process parameters for HRA, RA, CGHAZ area and BTA.

Of particular note is the formation of a larger CGHAZ area in the deep BD than in the shallow BD. The reason for this phenomenon is that the arc and molten metal contact a larger area when the bevel angle is larger, so that the solid metal phase easily conducts more heat to promote the formation of a coarse grained structure. These statements are consistent with the results in Ref. [28]. In addition, results from a previous study of intermediate gauge X70 steel [7] showed that TS was dominant for the CGHAZ area. In the current study, BD provided a more effective contribution to the CGHAZ area, and not TS.

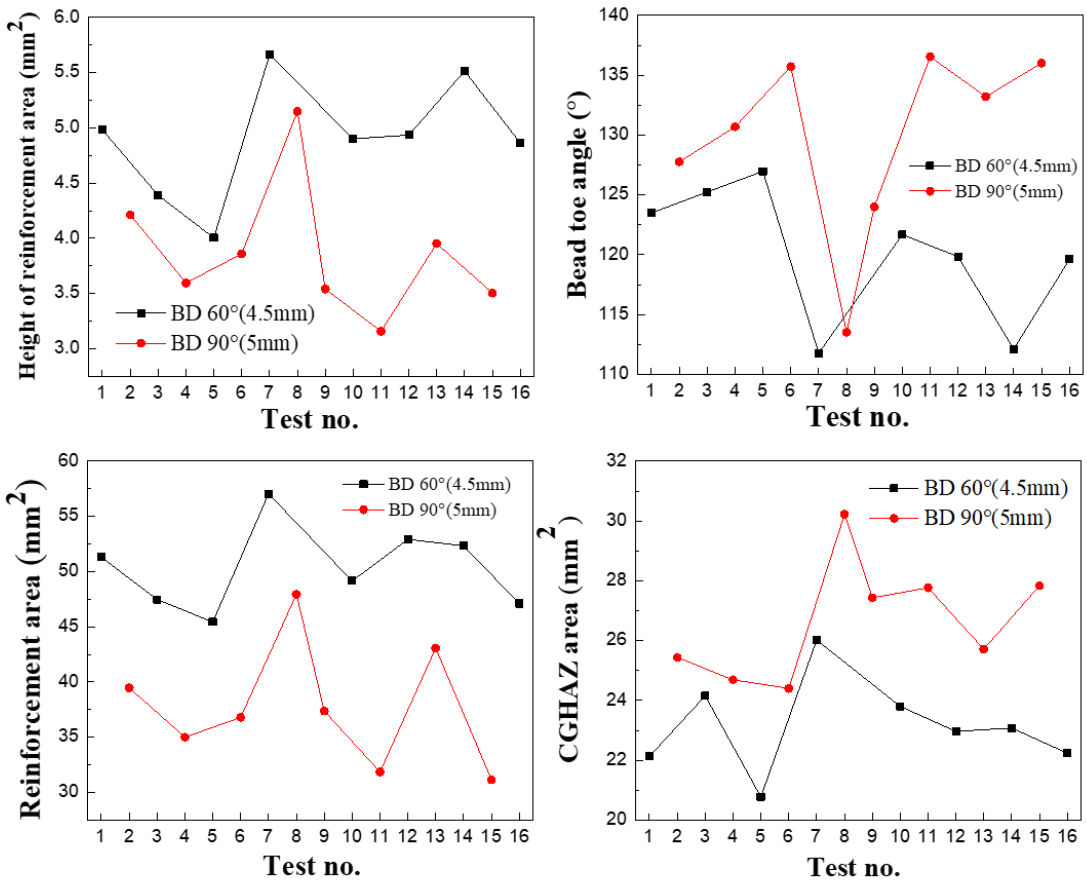

Figure 10 Measurements of RA, BTA, HRA and CGHAZ area for the two bevel specifications.

The BD had a smaller effect on the weld geometry ratio values (SPR and AR) and DIL than HI, V and TS, as shown in Figure 7. The values of SPR and AR were calculated from the BW. The smaller effect of BD on the BW can be explained in terms of the main liquid metal flow pattern and surface tension in the molten pool. The main flow pattern of liquid metal in the molten pool is liquid metal flowing upward along the boundary of the molten pool and colliding at the top of the weld, whereupon the liquid metal changes direction and descends into the pool [28].

The main flow pattern of liquid metal and surface tension are governed by the BW and they are affected by active elements, such as O, S, Si and Ni, dissolved in the liquid mixture metal [28, 30]. The BW is controlled by the surface tension force since it pulls liquid metal towards the center of the weld pool, which is varied by the concentration of the active elements. Another study

reported that bead width depends on the concentration of surface active elements and the local temperature profile [31]. In this study, the composition of the base metal X70 steel, the electrodes and the granular flux are uniform and identical for all 16 fabricated weldments. This means that the main flow pattern, surface tension and BW were not altered even for different bevel angles and bevel depths. Therefore, the BD had little influence on the weld geometry ratio.

4.2 Nonlinear Relationship of CWTSAW

Three order multiple regression (TOMR) was used to analyze the nonlinear relationship of controllable variables (welding parameters) and the response factors (geometry results and micro-hardness profiles). In addition, the interactions of welding parameters and micro-hardness profiles in the CGHAZ and WM are considered in the nonlinear regression analysis. The empirical equations were developed using Minitab 18 with the form in Equation 6 [7].

$$y = C_0 + \sum_{i=1}^{7}(C_i \cdot x_i) + \sum_{i=1}^{7}(C_{ii} \cdot x_i^2) + \sum_{i=1}^{7}\sum_{i>j}^{7}\left(C_{ij} \cdot x_i \cdot x_j\right) + \sum_{i=1}^{7}(C_{iii} \cdot x_i^3) + \sum_{i=1}^{7}\sum_{j>i}^{7}\sum_{k>j}^{7}\left(C_{ijk} \cdot x_i \cdot x_j \cdot x_k\right) \quad (6)$$

where y is the response factor (geometry characteristics and micro-hardness profile) which was predicted by the controllable variable x_i (welding parameters and different interactive combinations); C_i, C_{ii}, C_{ij}, C_{iii} and C_{ijk} are the coefficients. In this study, the confidence level of TOMR in Minitab 18 was set at 90% which means that any controllable variables with a P value less than or equal to 0.1 are statistically significant and considered as predictors in empirical equations. For example, 8 predictors in the CGHAZ micro-hardness TOMR equation from a total of 72 possible predictors (individual welding parameters and interactions) were considered which resulted in a good fit.

$$\text{CGHAZ micro-hardness} = 112 + 1.86 \cdot \text{CWFS} + 298 \cdot \text{HIL} - 13.31 \cdot \text{VL} + 1.44 \cdot \text{TS} - 0.0327 \cdot \text{CWFS}^2 - 5.89 \cdot \text{HIL} \cdot \text{TS} + 0.264 \cdot \text{VL} \cdot \text{TS} + 0.000169 \cdot \text{CWFS}^3 \quad (7)$$

Of particular note is that squared and cubed predictors are only associated with CWFS in the CGHAZ micro-hardness equation. This appears to be the dominant effect contributed by cold wire addition in comparison with other TOMR equations. The other TOMR equations for HRA, RA, CGHAZ area, SPR and WM micro-hardness are shown in Appendix A.

The calculated values for HRA, RA, CGHAZ area, micro-hardness of the CGHAZ and WM are plotted against the observed values in Figure 11. To validate each equation, three (3) complementary tests were conducted and are included in Figure 11 (triangles). The weld table for these complementary tests is shown in Table 4. TOMR equations have been developed to correlate the weld geometry results and CGHAZ and WM micro-hardness with weld parameters for heavy gauge X70 steels in comparison with the previous study of intermediate gauge X70 steels [7]. In addition, the range of R^2 values is from 81.6% to 97.9% and the geometric characteristics of the three complementary tests with the varied welding parameters levels show good correlation with the observed values (Figure 11).

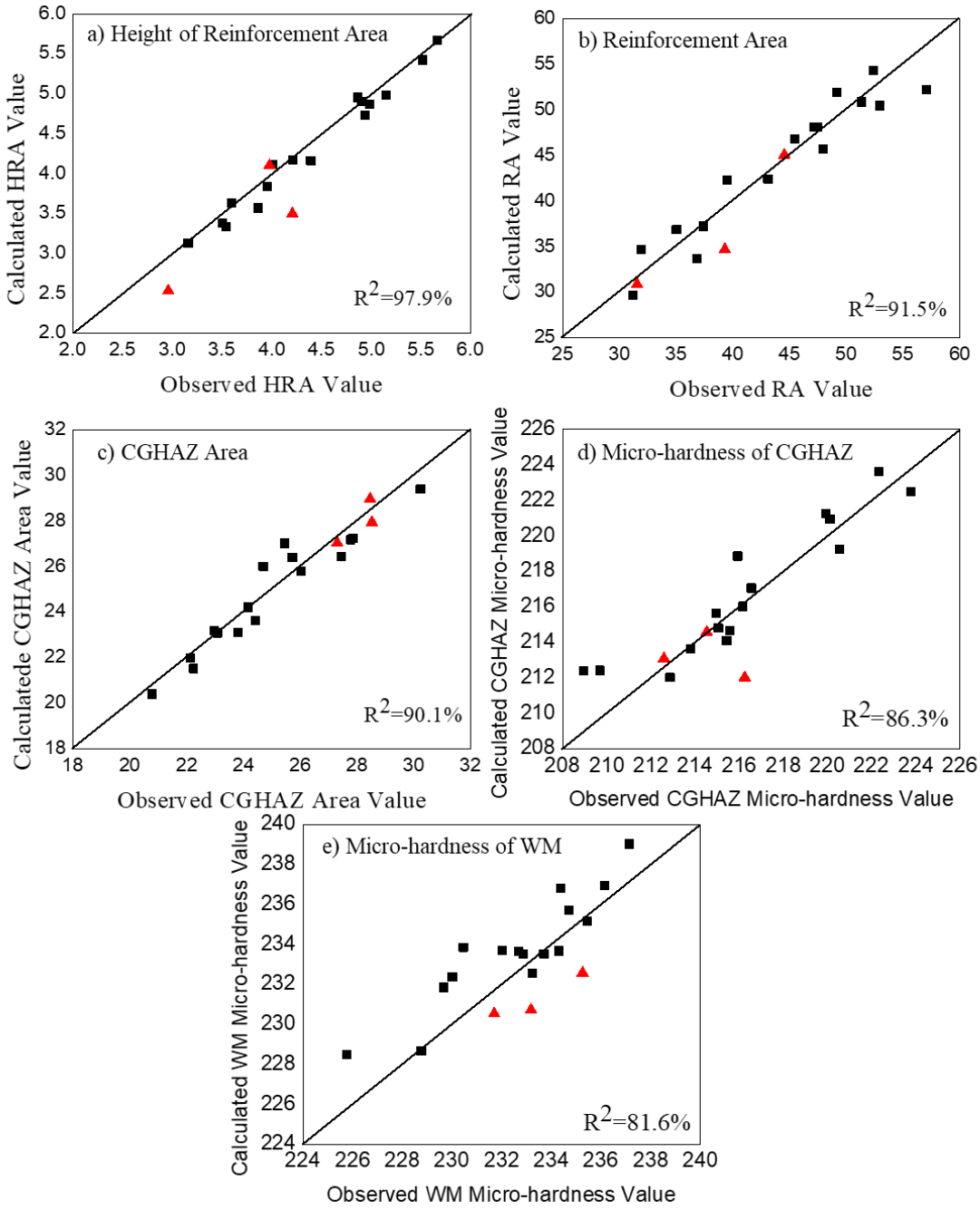

Figure 11 Observed and calculated values for the (a) HRA, (b) RA, (c) CGHAZ area, (d) micro-hardness of the CGHAZ and (e) micro-hardness of the WM. Complementary tests results are also shown (triangles).

4.3 Optimized Levels of CWTSAW

The S/N ratio was utilized to determine the optimized levels for each welding parameter. The welding parameters were categorized by two quality requirements, which are "lower-the-better" and "higher-the-better", respectively. AR, BTA, APR and BW are included in the "higher-the-better" quality requirements. DIL, CGHAZ area, HRA and RA are included in the "lower-the-better" quality requirements. The S/N ratio analysis was not conducted on the micro-hardness profiles since there was not agreement on which approach is better. The S/N ratio was calculated using Equations 8 and 9 [18].

$$\mathrm{S/N}_{(\mathrm{lower-the-bettter})} = -10\log_{10}\left(\frac{1}{n}\sum_{i=1}^{n} y_{ij}^{2}\right) \quad (8)$$

$$\mathrm{S/N}_{(\mathrm{higher-the-bettter})} = -10\log_{10}\left(\frac{1}{n}\sum_{i=1}^{n} \frac{1}{y_{ij}^{2}}\right) \quad (9)$$

where S/N is the signal-to-noise ratio, y_{ij} is the experimental value of the i th response characteristic in the jth test, and n is the number of tests.

A higher average S/N ratio value representing a given level of the weld parameter resulted in an optimal effect on the geometric characteristics, since higher S/N values mean lower noise effects [17, 32]. A weld parameter level with a higher S/N value is considered as the optimized parameter level, which results in an optimal effect on the geometric characteristics. The calculated S/N ratio values for the weld characteristics are shown in Appendix A (Table 10). Based on the calculated S/N ratio values,, the optimized levels for the CWTSAW parameters are summarized (Table 7). Overall, the optimal geometric characteristics are achieved using optimized levels of CWTSAW parameters; i.e., 1.6 kJ/mm for HIL (level 1), 1.3 kJ/mm for HIT (level 1), 21.2 mm/s for TS (level 1) and 25 mm^2 for BD (level 2).

Table 7 Optimized levels of CWTSAW parameters

Criteria	Characteristics	CWFS (mm/s)	HIL (kJ/mm)	HIT (kJ/mm)	VL (V)	VT (V)	TS (mm/s)	BD (mm^2)
Higher-the-better	BW	33.9	1.6	1.3	36	37	21.2	25
	AR	25.4	1.8	1.5	33	34	23.3	25
	BTA	16.9	1.6	1.3	36	37	21.2	25
	SPR	25.4	1.8	1.5	33	34	23.3	25
Lower-the-better	RA	33.9	1.8	1.3	36	37	21.2	25
	CGHAZ area	16.9	1.6	1.3	36	37	23.3	12
	DIL	25.4	1.6	1.3	33	34	21.2	25
	HRA	33.9	1.6	1.3	36	37	21.2	25

4.4 Comparison of TSAW and CWTSAW

Two heavy gauge X70 welds were produced by conventional TSAW and CWTSAW processes. Then, a comparison in terms of average micro-hardness and the phase fraction of MA constituents in the CGHAZ of TSAW and CWTSAW weld was undertaken. The weld testing conditions are shown in Table 8. The HIL, HIT, VL, VT, TS and BD for both the TSAW and CWTSAW weld are identical and only the CWFS is varied.

Table 8 Welding condition of TSAW and CWTSAW

Process type	CWFS (mm/s)	HIL (kJ/mm)	HIT (kJ/mm)	VL (V)	VT (V)	TS (mm/s)	BD (mm^2)
TSAW	0	1.6	1.3	31	34	21.2	25
CWTSAW	16.9	1.6	1.3	31	34	21.2	25

The approach to micro-hardness measurements followed the schematic description in Figure 4. Figure 12 shows that the average micro-hardness values measured in the CGHAZ of the TSAW and CWTSAW welds. The hardness is higher for the CGHAZ of the TSAW weld than for

the CWTSAW weld. The lower hardness distribution in the CGHAZ of the CWTSAW weld is closely related to the microstructure modification due to heat reduction by heat consumption of the cold wire addition.

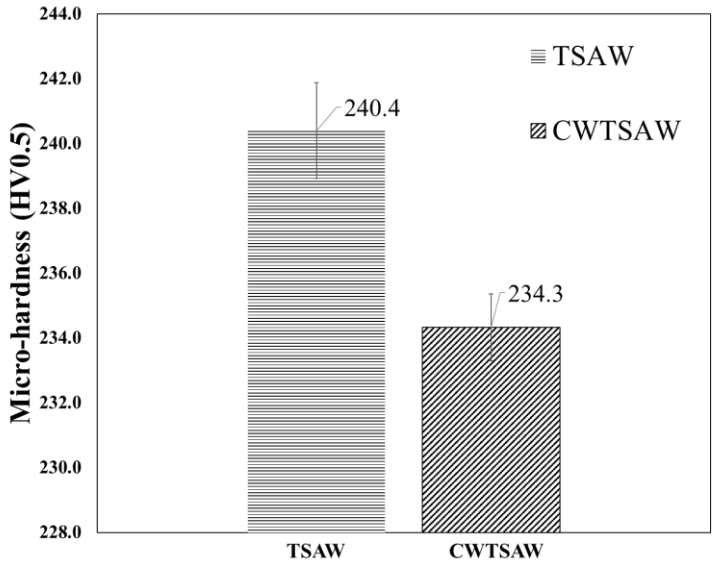

Figure 12 Average micro-hardness values in the CGHAZ for TSAW and CWTSAW.

Optical and SEM SE micrographs of MA constituents in the CGHAZ of TSAW and CWTSAW samples are shown in Figure 13. The MA constituents appear as shiny white features in the optical and SEM images after etching with the modified LePera's etchant [21]. White linear segments are visible in the SEM images, since some of the MA constituents were formed at the grain boundaries. The MA fractions from the optical micrographs (Figures 13a and 13c) are 5.3% (0.2%) and 2.8% (0.1%) for the TSAW and CWTSAW welds, respectively. The MA fractions in the CGHAZ determined from the SEM micrographs (Figures 13b and 13d) are 5.7% (0.2%) and 3.3% (0.2%) for TSAW and CWTSAW samples, respectively. The values in the brackets represent one standard deviation.

In terms of the morphology of MA constituents, the MA regions in the TSAW sample from both optical and SEM SE micrographs are mainly massive and the MA constituents of the TSAW sample are more elongated and larger than those in the CWTSAW sample. The MA features in the CWTSAW sample are finer and more dispersed (Figures 13c and 13d) than those in the TSAW sample (Figures 13a and 13b). The average micro-hardness in the CGHAZ of TSAW samples is higher than that in the CWTSAW sample, which can be correlated with the higher MA constituents fraction and the different MA morphology (blocky and elongated) in the TSAW sample.

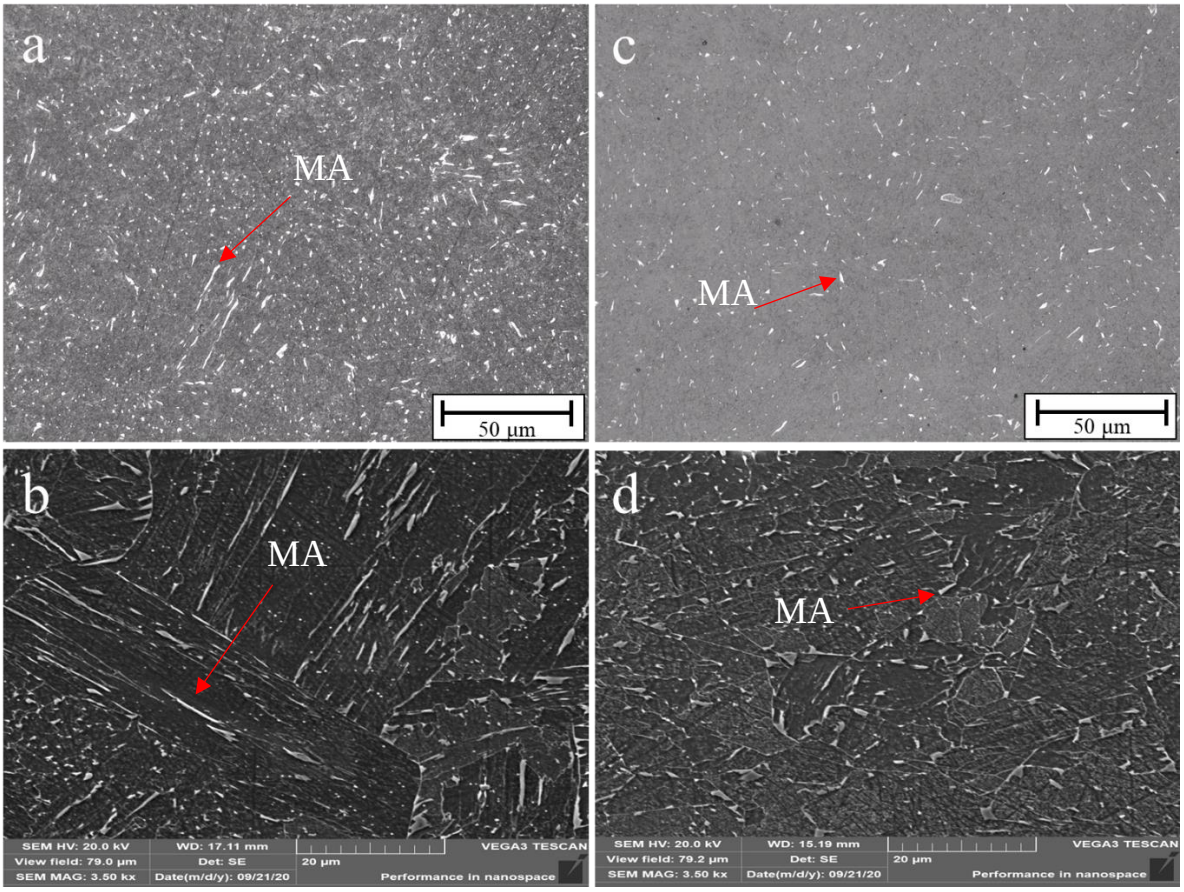

Figure 13 Weld samples fabricated by TSAW (a, b) and CWTSAW (c, d) showing MA constituents (shiny white features) in the CGHAZ. Images a and c are optical micrographs, while images b and d are SEM SE micrographs.

Denser MA regions with elongated MA constituents that formed in the CGHAZ resulted in localized brittle zones (LBZs). Luo et al. [33] and Mohammadijoo et al. [10, 34] reported that the formation of LBZs can cause initiation and propagation of cleavage fracture at the PAG boundaries in the HAZ, deteriorating the fracture toughness. There are elongated MA constituents and a higher overall MA fraction in the CGHAZ of the TSAW samples than in the CWTSAW samples. This can be interpreted as the reason for the higher hardness in the CGHAZ of the TSAW samples. In addition, fine and more dispersed MA constituents in the CGHAZ of the CWTSAW samples inhibit the formation of LBZs. This change in MA morphology is strongly related to the cold wire addition reducing the overall heat input by consuming heat from the molten pool.

5.0 Conclusions

To meet the essential upgrade of X70 pipeline steel in heavy gauge pipes, the effect of cold wire tandem submerged arc welding (CWTSAW) parameters and bevel design on the change in weld geometry and micro-hardness of heavy gauge X70 (19.1 mm) was investigated and the input levels of welding parameters were optimized. The following general conclusions can be made:

1. Cold wire feed speed had the most dominant effect on micro-hardness profiles, since the cold wire addition altered the local thermal cycle by consuming heat from the molten pool. Cold wire addition can restrain the increase in overall heat input of conventional tandem submerged arc welding in heavy gauge pipe making.
2. Geometry changes, including the reinforcement size and CGHAZ area, are sensitive to the bevel design due to the achievement of full penetration, but the bevel design only had a minor effect on the weld metal and CGHAZ micro-hardness.
3. Predictive equations for micro-hardness values of the CWTSAW sample were developed using three order multiple regression analysis and showed good correlation in contrast to previous work.
4. A CWTSAW process, with an overall nominal heat input of 2.9 kJ/mm (lead + trail electrode), a travel speed of 21.2 mm/s, a bevel angle of 90° and a bevel depth of 5 mm, reduced the CGHAZ area, dilution and reinforcement size.
5. The CWTSAW samples had lower martensite-austenite (MA) fractions with fine and dispersed MA constituents resulting in the lower micro-hardness values in the CGHAZ. This type of MA morphology, which is due to the lower actual heat input introduced to the weld pool, inhibits the formation of local brittle zone in the CGHAZ of CWTSAW sample.

Acknowledgments

The authors would like to acknowledge the Natural Sciences and Engineering Research Council (NSERC) of Canada, Evraz Inc. NA and TC Energy Corp. for providing financial support. Special thanks are also in order for the Research and Development Division of Evraz Inc. NA for providing welding equipment and technical assistance to conduct welding tests.

Data availability All data generated or analyzed during this study are included in this published article.

Code availability Not applicable

Funding This research was financially supported by the Natural Sciences and Engineering Research Council (NSERC) of Canada, Evraz Inc. NA and TC Energy Corp.

Declarations

Ethics approval Not applicable.

Consent to participate Not applicable.

Consent for publication Not applicable.

Conflict of interest The authors declare no competing interests.

Appendix

ANOVA tables, average signal-to-noise (S/N) ratio and empirical equations from TOMR analysis.

Table 9 ANOVA results for eight weld characteristics and micro-hardness profile

Characteristic		CWFS	HIL	HIT	VL	VT	TS	BD	R^2
BW	DF	3	1	1	1	1	1	1	82.2%
	SS	0.74	0.48	0.23	5.28	0.87	3.84	0.11	
	F	0.59	1.16	0.54	12.64	2.08	9.17	0.26	
	P	0.65	0.32	0.49	0.012	0.20	0.02	0.63	
HRA	DF	3	1	1	1	1	1	1	97.8%
	SS	0.63	0.01	0.64	0.73	1.51	0.92	4.28	
	F	6.40	0.16	19.43	22.19	46.02	28.14	130.72	
	P	0.03	0.70	0.01	0.00	0.00	0.00	0.00	
BTA	DF	3	1	1	1	1	1	1	89.0%
	SS	50.03	8.56	180.71	112.79	108.68	82.23	367.83	
	F	0.89	0.46	9.64	6.01	5.79	4.38	19.61	
	P	0.50	0.52	0.02	0.05	0.05	0.08	0.00	
RA	DF	3	1	1	1	1	1	1	95.2%
	SS	40.06	1.23	69.53	15.26	134.62	16.04	626.04	
	F	1.76	0.16	9.19	2.02	17.79	2.12	82.72	
	P	0.25	0.70	0.02	0.21	0.01	0.20	0.00	
CGHAZ area	DF	3	1	1	1	1	1	1	93.1%
	SS	4.90	10.76	8.34	8.37	4.01	1.57	50.19	
	F	1.50	9.87	7.65	7.68	3.68	1.44	46.04	
	P	0.31	0.02	0.03	0.03	0.10	0.28	0.001	

Table 9 (continued)

Characteristic		CWFS	HIL	HIT	VL	VT	TS	BD	R^2
AR	DF	3	1	1	1	1	1	1	89.2%
	SS	0.01	0.03	0.03	0.06	0.01	0.05	0.01	
	F	0.68	6.54	7.58	14.86	3.71	11.32	3.46	
	P	0.59	0.04	0.03	0.01	0.10	0.02	0.11	
SPR	DF	3	1	1	1	1	1	1	84.4%
	SS	0.01	0.012	0.005	0.015	0.001	0.04	0.001	
	F	1.27	4.68	1.93	5.76	0.38	15.54	0.42	
	P	0.37	0.07	0.21	0.05	0.56	0.01	0.54	
Dilution	DF	3	1	1	1	1	1	1	81.9%
	SS	0.0002	0.002	0.0001	0.0001	0.0013	0.0002	0	
	F	0.4	12.94	0.95	0.69	9.64	1.76	0	
	P	0.76	0.01	0.37	0.44	0.02	0.23	1.00	
CGHAZ Hardness	DF	3	1	1	1	1	1	1	68.1%
	SS	115.57	19.78	2.25	10.35	0.50	27.28	0.66	
	F	2.80	1.44	0.16	0.75	0.04	1.98	0.05	
	P	0.13	0.28	0.70	0.42	0.86	0.21	0.83	
WM Hardness	DF	3	1	1	1	1	1	1	75.6%
	SS	38.64	1.28	38.28	0.02	11.46	11.94	0.52	
	F	2.37	0.24	7.03	0.00	2.10	2.19	0.10	
	P	0.17	0.65	0.04	0.95	0.20	0.19	0.77	

Table 10 Average signal-to-noise (S/N) ratio for seven welding parameters of CWTSAW

Symbol	Parameters	Level	BW	HRA	BTA	RA
A	CWFS	1	23.0 (0.3)	-12.6 (0.6)	**42.1 (0.1)**	-32.6 (0.8)
		2	22.8 (0.4)	-13.3 (0.8)	41.7 (0.4)	-33.3 (0.8)
		3	**23.1 (0.2)**	**-12.2 (0.9)**	41.9 (0.3)	**-32.5 (0.9)**
		4	22.8 (0.4)	-12.9 (0.9)	41.9 (0.40)	-32.6 (0.9)
B	HIL	1	**23.0 (0.2)**	**-12.5 (0.5)**	**42.0 (0.2)**	-32.9 (0.4)
		2	22.8 (0.2)	-12.7 (0.7)	41.9 (0.2)	**-32.6 (0.7)**
C	HIT	1	**23.0 (0.2)**	**-12.3 (0.5)**	**42.2 (0.2)**	**-32.3 (0.6)**
		2	22.8 (0.3)	-13.1 (0.6)	41.7 (0.2)	-33.2 (0.5)
D	VL	1	22.6 (0.2)	-12.3 (0.5)	41.7 (0.2)	-32.9 (0.6)
		2	**23.3 (0.2)**	**-12.2 (0.5)**	**42.1 (0.2)**	**-32.6 (0.6)**
E	VT	1	22.8 (0.2)	-13.3 (0.6)	41.7 (0.2)	-33.3 (0.6)
		2	**23.1 (0.2)**	**-12.2 (0.4)**	**42.1 (0.2)**	**-32.2 (0.5)**
F	TS	1	**23.2 (0.2)**	**-12.2 (0.6)**	**42.1 (0.2)**	**-32.5 (0.7)**
		2	22.6 (0.2)	-13.2 (0.5)	41.8 (0.2)	-33.0 (0.5)
G	BD	1	22.9 (0.2)	-13.8 (0.3)	41.6 (0.2)	-34.0 (0.2)
		2	**23.0 (0.2)**	**-11.7 (0.5)**	**42.2 (0.2)**	**-31.5 (0.5)**

*Higher S/N ratio values are indicated in bold and values in brackets indicate one standard deviation.

Table 10 (Continued)

Symbol	Parameters	Level	SPR	CGHAZ area	Dilution	AR
A	CWFS	1	-1.0 (0.3)	**-27.6 (0.3)**	3.6 (0.2)	-1.0 (0.5)
		2	**-0.7 (0.6)**	-28.0 (0.7)	**3.7 (0.1)**	**-0.6 (1.0)**
		3	-1.3 (0.2)	-28.1 (0.4)	3.6 (0.1)	-0.9 (0.2)
		4	-1.2 (0.5)	-27.8 (0.5)	3.5 (0.1)	-0.7 (0.4)
B	HIL	1	-1.3 (0.2)	**-27.6 (0.3)**	**3.7 (0.1)**	-1.2 (0.4)
		2	**-0.8 (0.3)**	-28.2 (0.3)	3.5 (0.1)	**-0.4 (0.4)**
C	HIT	1	-1.2 (0.1)	**-27.6 (0.3)**	**3.6 (0.1**)	-1.2 (0.3)
		2	**-0.9 (0.4)**	-28.2 (0.3)	3.5 (0.1)	**-0.4 (0.4)**
D	VL	1	**-0.8 (0.3)**	-28.1 (0.3)	**3.6 (**0.1)	**-0.2 (0.4)**
		2	-1.3 (0.2)	**-27.7 (0.3)**	3.5 (0.1)	-1.4 (0.3)
E	VT	1	**-1.0 (0.3)**	-28.1 (0.3)	**3.7 (0.1)**	-0.5 (0.4)
		2	-1.1 (0.2)	**-27.7 (0.3)**	3.5 (0.1)	**-1.1 (0.3)**
F	TS	1	-1.5 (0.2)	-28.0 (0.3)	**3.7 (0.1)**	-1.3 (0.3)
		2	**-0.6 (0.2)**	**-27.9 (0.3)**	3.5 (0.1)	**-0.3 (0.4)**
G	BD	1	-1.1 (0.2)	**-27.3 (0.2)**	3.6 (0.1)	-1.1 (0.4)
		2	**-1.0 (0.4)**	-28.5 (0.2)	**3.7 (0.1)**	**-0.5 (0.4)**

*Higher S/N ratio values are indicated in bold and values in brackets indicate one standard deviation.

Developed empirical equations from TOMR analysis:

WM micro-hardness = 18 - 0.398· CWFS + 137· HIT +11.79· VT - 4.02· TS + 0.00251· $CWFS^2$ – 8.02· HIT· VT + 3.12· HIT· TS

HRA = -284 + 9·VL + 8 · VT + 29 · BD - 0.3 · VL · VT - 0.9 · VL · BD - 0.8 · VT · BD - 0.002 · HIL · VT · BD + 0.02 · VL · VT · BD + 0.004 · CWFS · HIT^2 + 0.00003 · CWFS · BD^2 + 0.4 · HIL^2 · HIT

RA = 61 - 0.014 · HIL · VL · BD + 0.021 · HIT · TS · BD - 0.0013 · VT^2 · BD

CGHAZ area = 0.56 + 8.2 · HIL · HIT + 0.9 · HIL · BD + 0.9 · HIT · BD - 0.78 · HIL · HIT · BD - 0.0006 · VL · VT · BD

References

1. Collins LE, Dunnett K, Hylton T, Ray A (2018) Development of heavy gauge X70 helical line pipe. In: Proceedings of the 2018 12th International Pipeline Conference (IPC), Calgary, Alberta, Canada

2. Weman K (2012) Welding Processes Handbook (2nd Edition) - 10.4.2 Welding Parameters and Weld Quality, Woodhead Publishing in Materials. In: Weman K (ed) Welding Processes Handbook (2nd Edition). Woodhead Publishing, Paperback ISBN: 9780857095107, eBook ISBN: 9780857095183, pp 105–106

3. Bortsov AN, Shabalov IP, Velichko AA, et al (2013) Features of multi-electrode submerged-arc welding in the production of high-strength thick-walled pipes. Metallurgist 57:310–319. https://doi.org/10.1007/s11015-013-9730-0

4. Moeinifar S, Kokabi AH, Madaah Hosseini HR, et al (2010) Influence of four wires tandem submerged arc welding process on heat affected zone properties in high strength pipeline steel. Proc 2010 Int Conf Mech Ind Manuf Technol MIMT 2010 85–89. https://doi.org/10.1115/1.859544.paper14

5. Far SM (2012) Influence of thermal simulated and real tandem submerged arc welding process on the microstructure and mechanical properties of the coarse grained heat affected zone. Appl Mech Mater 110–116:3191–3198. https://doi.org/10.4028/www.scientific.net/AMM.110-116.3191

6. Mruczek MF, Parker D (2006) Cold Wire Feed Submerged Arc Welding. Concurrent Technologies Corporation, Johnstown, PA

7. Mohammadijoo M, Kenny S, Collins L, et al (2017) Influence of cold-wire tandem submerged arc welding parameters on weld geometry and microhardness of microalloyed pipeline steels. Int J Adv Manuf Technol 88:2249–2263. https://doi.org/10.1007/s00170-016-8910-z

8. Ramakrishnan Mannarsamy*, S.K.Shrivastava*, PiyushThakor*, Gautam Chauhan* SKJ, Korada* and R korada (2015) Establishment of cold wire addition technology in multiwire submerged arc welding for line pipe manufacturing to improve the weldment quality. ASME 2015 India Oil Gas Pipeline Conf 1–11

9. Júnior RC, Esteves L, Santos NF, et al (2019) Influence of Heat Input and Cold Wire Feeding Rate on Pitting Corrosion Resistance of Submerged Arc Welding Duplex Stainless Steel Welds. J Mater Eng Perform 28:1969–1976. https://doi.org/10.1007/s11665-019-03967-7

10. Mohammadijoo M, Collins L, Lazor R, et al (2018) Influence of Cold-Wire Submerged Arc Welding on the Toughness of Microalloyed Steel. Weld J 97:338s-352s. https://doi.org/10.29391/2018.97.029

11. Mohammadijoo M, Collins L, Henein H, Ivey DG (2017) Evaluation of cold wire addition effect on heat input and productivity of tandem submerged arc welding for low-carbon microalloyed steels. Int J Adv Manuf Technol 92:817–829. https://doi.org/10.1007/s00170-017-0150-3

12. Ishigami A, Roy MJ, Walsh JN, Withers PJ (2017) The effect of the weld fusion zone shape on residual stress in submerged arc welding. Int J Adv Manuf Technol 90:3451–3464. https://doi.org/10.1007/s00170-016-9542-z

13. Taguchi G (1993) Taguchi on Robust Technology Development: Bringing Quality Engineering Upstream. ASME Press ISBN-10: 0791800288, https://doi.org/10.1115/1.800288

14. Tarng YS, Yang WH (1998) Application of the Taguchi method to the optimization of the submerged arc welding process. Mater Manuf Process 13:455–467. https://doi.org/10.1080/10426919808935262

15. Sarkar A, Roy J, Majumder A, Saha SC (2014) Optimization of Welding Parameters of Submerged Arc Welding Using Analytic Hierarchy Process (AHP) Based on Taguchi Technique. J Inst Eng Ser C 95:159–168. https://doi.org/10.1007/s40032-014-0114-4

16. Roy RK (2010) Primer on the Taguchi Method (2nd Edition) - 6. Analysis of Variance (ANOVA). In: Roy RK (ed) Primer on the Taguchi Method, 2nd ed. Society of Manufacturing Engineers (SME)

17. Mathews P (2004) Chapter 8 Linear Regression. In: Design of Experiments with MINITAB. American Society for Quality (ASQ), pp 273–346

18. Mason RL, Gunst RF, Hess JL (2003) Analysis of Nested Designs and Designs for Process Improvement. In: Statistical Design and Analysis of Experiments - With Applications to Engineering and Science, 2nd Editio. pp 423–458

19. ASTM (2017) E3-11: Stardard Guide for Preparation of metallographic specimens. 11:1–17

20. ASTM (2017) E384-17: Standard Test Method for Microindentation Hardness of Materials. ASTM Int. 1–40

21. Mohammadijoo M, Henein H, Ivey DG (2016) Microstructural characterization of the HAZ in welded microalloyed steels. In: Microscopy Society of Canada 2016 MSC/SMC 43rd Annual Meeting. Edmonton, Alberta, Canada

22. Reisgen U, Dilthey U, Aretov I (2008) SAW cold wire technology - Economic alternative for joining hot crack sensitive nickel-base alloys. Hot Crack Phenom Welds II 215–237. https://doi.org/10.1007/978-3-540-78628-3_12

23. Murugan N, Parmar RS, Sud SK (1993) Effect of submerged arc process variables on dilution and bead geometry in single wire surfacing. J Mater Process Tech 37:767–780. https://doi.org/10.1016/0924-0136(93)90135-S

24. Shahverdi Shahraki H, Mozafari H (2015) Modeling and Optimizing of Submerged Arc Welding Process by Taguchi Design of Experiments in Presence of Magnesium Oxide Nano-Particles. Appl Mech Mater 763:52–57. https://doi.org/10.4028/www.scientific.net/amm.763.52

25. O'Brien A (2004) Welding Handbook. Volume 2: Welding Processes, Part 1 - 6.5 Process variables. In: 9th Editio. American Welding Society (AWS), ISBN:

9780871717290/0871717298, pp 278–282, ISBN: 9780871717290/0871717298

26. Pepin J, Penniston C, Henein H, et al (2012) Using semipenetration ratio to characterize effects of waveform variables on bead profile and heat affected zone with single electrode submerged arc welding. Can Metall Q 51:284–293. https://doi.org/10.1179/1879139512Y.0000000018

27. Sun Z, Pan D, Kuo M (2002) High Productivity Cladding with Non-Consumable Electrode Arc Processes. In: 6'th International Trendsin Welding Research Conference Proceedings, 15-19 April 2002, Pine Mountain, GA, USA, ASM International. ASM International, pp 436–441

28. Chen J, Schwenk C, Wu CS, Rethmeier M (2012) Predicting the influence of groove angle on heat transfer and fluid flow for new gas metal arc welding processes. Int J Heat Mass Transf 55:102–111. https://doi.org/10.1016/j.ijheatmasstransfer.2011.08.046

29. Huang Y, Yu H, Zhang J, Ren C (2019) Study on arc physical characteristics of GPCA-TIG welding under different angles of V groove. Eng Res Express 1:015032. https://doi.org/10.1088/2631-8695/ab3c04

30. Ribic B, Tsukamoto S, Rai R, DebRoy T (2011) Role of surface-active elements during keyhole-mode laser welding. J Phys D Appl Phys 44:. https://doi.org/10.1088/0022-3727/44/48/485203

31. Rajesh Kannan P, Muthupandi V, Devakumaran K (2018) On the effect of temperature coefficient of surface tension on shape and geometry of weld beads in hot wire gas tungsten arc welding process. Mater Today Proc 5:7845–7852. https://doi.org/10.1016/j.matpr.2017.11.465

32. Gowthaman K, Saiganesh J, Rajamanikam C (2013) Determination of submerged arc welding process parameters using Taguchi method and regression analysis. In: 2013 International Conference on Energy Efficient Technologies for Sustainability. IEEE, Nagercoil, India, pp 842–847

33. Luo X, Chen X, Wang T, et al (2018) Effect of morphologies of martensite–austenite constituents on impact toughness in intercritically reheated coarse-grained heat-affected zone of HSLA steel. Mater Sci Eng A 710:192–199. https://doi.org/10.1016/j.msea.2017.10.079

34. Mohammadijoo M, Valloton J, Collins L, et al (2018) Characterization of martensite-austenite constituents and micro-hardness in intercritical reheated and coarse-grained heat affected zones of API X70 HSLA steel. Mater Charact 142:321–331. https://doi.org/10.1016/j.matchar.2018.05.057